Colloids and Surfaces A 604 (2020) 125315

Contents lists available at ScienceDirect

Colloids and Surfaces A

journal homepage: www.elsevier.com/locate/colsurfa

Reductive immobilization of uranium by stabilized zero-valent iron nanoparticles: Effects of stabilizers, water chemistry and long-term stability

Xiao Zhao[a,b,*], Wen Liu[b,c], Zhengqing Cai[b], Jie Fu[b], Jun Duan[b], Dongye Zhao[b,**], Michael Bozack[d], Yucheng Feng[e]

[a] College of Water Resources & Civil Engineering, China Agricultural University, Beijing 100083, China
[b] Environmental Engineering Program, Department of Civil Engineering, Auburn University, Auburn, AL 36849, USA
[c] The Key Laboratory of Water and Sediment Sciences, Ministry of Education; College of Environmental Sciences and Engineering, Peking University, Beijing 100871, China
[d] Department of Physics, Auburn University, AL 36849, USA
[e] Department of Crop, Soil and Environmental Sciences, Auburn University, AL 36849, USA

GRAPHICAL ABSTRACT

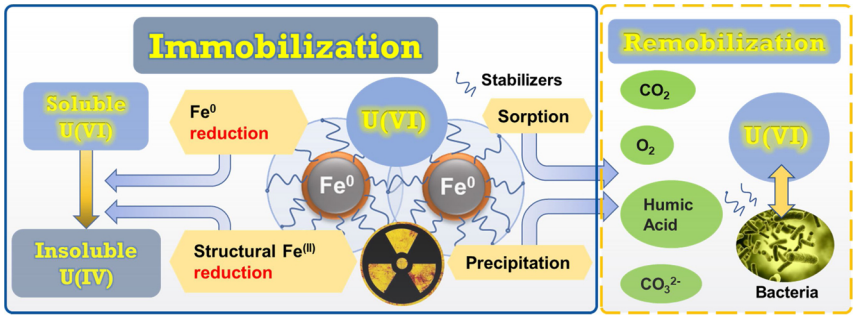

ARTICLE INFO

Keywords:
Zero valent iron
Radionuclide
Reductive immobilization
Stabilized nanoparticle
Uranium immobilization

ABSTRACT

Uranium is one of the most commonly detected radionuclides in the environment. Of the two most predominant oxidation states, U(VI) is much more soluble, mobile and toxic than U(IV). Consequently, converting U(VI) to U (IV) can facilitate the removal of U from water and reduce its mobility and biological exposure. In this work, stabilized zero-valent iron (ZVI) nanoparticles were prepared using starch or carboxymethyl cellulose (CMC) as stabilizers and then tested for reductive removal of U(VI) from simulated groundwater. Nearly 100% removal of U(VI) (initial U = 25 mg/L) was achieved using CMC-stabilized ZVI (Fe = 35 mg/L) at pH 6. In pH range of 6–9, the lower pH favored the reaction. CMC-ZVI nanoparticles presented better deliverability than starch-ZVI, while bare ZVI nanoparticles was almost trapped in the soil column. CMC-ZVI worked effectively in the presence of a model humic acid (up to 10 mg/L as TOC) and bicarbonate (1 mM), though higher dosages of the ligands inhibited U(VI) removal. After treatment, no re-mobilization of U was detected when aged for 6 months under anoxic conditions and the addition of strong ligands only remobilized U(VI). When exposed to oxic conditions, the immobilized U will be partially oxidized and remobilized due to the ingress of atmospheric O_2 and CO_2. In terms of toxicity reduction, the ZVI treated U had almost no inhibition for natural bacteria activity, while

* Corresponding author at: College of Water Resources & Civil Engineering, China Agricultural University, Beijing 100083, China.
** Corresponding author at: Environmental Engineering Program, Department of Civil Engineering, Auburn University, Auburn, AL 36849, USA.
E-mail addresses: xiaozhao88@cau.edu.cn (X. Zhao), zhaodon@auburn.edu (D. Zhao).

https://doi.org/10.1016/j.colsurfa.2020.125315
Received 5 June 2020; Received in revised form 10 July 2020; Accepted 18 July 2020
Available online 04 August 2020
0927-7757/ © 2020 Elsevier B.V. All rights reserved.

dissolved U(VI) showed significant inhibitive effects. The CMC-ZVI nanoparticles may serve as effective reactive materials to facilitate immobilization of U(VI) in groundwater, which in turn can greatly mitigate the human exposure and toxic effects of U on biota.

1. Introduction

Uranium (U) is one of the most widely detected radionuclides at sites associated with nuclear material mining, nuclear energy production, nuclear weapon tests and radioactive material disposal [1]. For instance, more than 10 billion gallons of groundwater were reported to be contaminated by U mill tailings in the U.S. by 1996. In addition, U was detected in groundwater at 12 of the 18 major Department of Energy (DOE) facilities with concentrations ranging from 0.001 to 1700 000 μg/L [2]. U in groundwater can invade into the food chain, resulting in various health effects including cancer, kidney and liver damages [3].To mitigate human exposure, the U.S. Environmental Protection Agency (USEPA) has established a maximum contaminant level (MCL) of 30 μg/L for U in drinking water [3].

Like many other redox-active metals and radionuclides (e.g., Cr, As, Se, and Tc), the environmental impacts and mobility of U are strongly governed by the redox conditions. In most soil-groundwater systems, U exits primarily in the hexavalent U(VI) and tetravalent U(IV) [1]. Under oxic conditions, the predominant form is U(VI), which is soluble and can form stable complex with carbonate resulting in increased mobility (Blake et al., 1956). Under an reducing environment, however, the reduction of U(VI) to U(IV) leads to the formation of sparingly soluble uraninite (UO_2) ($\log K_{sp} = 4.832$) [4]. Therefore, reductive transformation of U(VI) to U(IV) has been proposed as a promising technique to remove/immobilize U(VI) in groundwater. In addition, the mobility of uranium in the subsurface can be influenced by several factors including pH, redox potential, temperature, soil texture, and organic and inorganic compounds [1,5]. In the typical natural groundwater pH range (5.0–9.0), U(VI) exists predominantly in the soluble and stable hydrolyzed forms [1]. Humic acid (HA) exists in natural water body from a few mg/L to more than a few hundred mg/L as dissolved organic carbon (DOM) [6]. HA can form strong complexes with U, resulting in an increased solubility and mobility of U in groundwater. In carbonate-containing water, U(VI) is present as a series of aqueous carbonate complexes [1]. However, the influence of HA and bicarbonate on U(VI) reduction by stabilized zero valent iron (ZVI) nanoparticles have not been studied.

Various studies have demonstrated that reductive immobilization of U(VI) can be achieved by reducing media such as mixed ferrous/ferric hydroxides [7], goethite, lepidocrocite, mackinawite [8], amorphous iron sulfide [9], hydrogen sulfide [10], sulfide minerals [11], sulfate-reducing bacteria [12] and bare ZVI particles [13]. Of these materials, ZVI aggregates have been widely tested for reductive immobilization of redox sensitive metals, metalloids and radionuclides [14]. Gu et al. found that ZVI filings provided faster reaction kinetics and higher efficiency for U(VI) removal compared to peat and iron oxides, and the researchers confirmed that U(IV) precipitates were formed on the ZVI surface [15]. More recently, Yan et al. reported that bare ZVI nanoparticles removed U(VI) 5 times faster than conventional iron flings owing to the greater specific surface area and reactivity [13], and the X-ray photoelectron spectroscopy (XPS) results confirmed that reductive conversion of U(VI) to U(IV) was the key mechanism through analyses.

However, ZVI nanoparticles prepared through the borohydride reduction method tend to aggregate rapidly (in minutes), which greatly curbs their unique advantages of high reactivity and soil mobility. To prevent particle aggregation, a number of particle stabilization techniques have been developed and well summarized in a recent review [14]. Of the various stabilizers reported so far, polysaccharides, such as starch and carboxymethyl cellulose (CMC), have attracted great attention due to their high particle stabilizing effectiveness, low-cost and environmental compatibility [16,17]. Extensive lab and field tests showed that the stabilized ZVI nanoparticles offer not only much greater reactivity, but much improved soil deliverability [16–18]. When applied for U(VI), we hypothesized that stabilized ZVI nanoparticles, once delivered into the subsurface, are able to effectively reduce the soluble U(VI) to insoluble U(IV), thereby achieving *in situ* reductive immobilization of U(VI) in soil and groundwater.

To be practically viable, it is critical to understand the potential of remobilization of U after treatment. A perturbation in the local environmental conditions may remobilize and oxidize the treated U. For instance, the presence of elevated natural ligands (HA and/or bicarbonate) in the groundwater may complex with adsorbed U(VI), resulting in remobilization. In addition, microbial activities and biogeochemical interactions may also induce oxidation and remobilization. Studies on the microorganisms in U contaminated sites indicated that the local bacteria may influence the U mobility through complexation and redox reactions [19]. While soluble U(VI) has been found toxic to many microorganisms [20,21], several sulfate-reducing bacteria (such as *Shewanella*, *Geobacter* and *Desulfovibrio* species) and iron-reducing bacteria (DIRB—*Geobacter* and *Pyrobaculum* species) were demonstrated to be able to reductively immobilize U(VI) [1]. Yet, the interactions between ZVI-immobilized U and common bacteria under typical groundwater conditions remains unclear.

The overall goal of this research was to test the feasibility of stabilized ZVI nanoparticles for reductive immobilization of U(VI) in soil and groundwater, and to examine the stability of immobilized U under various biogeochemical conditions. Specifically, this work aimed to: 1) test the effectiveness of the stabilized ZVI nanoparticles for immobilization of U(VI); 2) explore the effects of the stabilizers and pH; 3) examine the effects of typical groundwater conditions, such as DOM and bicarbonate; 4) investigate the remobilization potential of treated U under various geochemical and biological conditions; and 5) elucidate the underlying U(VI) immobilization and remobilization mechanisms.

2. Materials and methods

2.1. Chemicals

The following chemicals (analytical grade or higher) were used as received: ferrous sulfate heptahydrate ($FeSO_4{\cdot}7H_2O$, Acros Organics, Morris Plains, NJ, USA), sodium carboxymethyl cellulose (MW = 90 000, degree of substitute = 0.7, Acros Organics), Tris (hydroxymethyl) aminomethane (Tris buffer, Acros Organics), a water-soluble potato starch (Sigma-Aldrich, Milwaukee, WI, USA), sodium borohydride ($NaBH_4$, ICN Biomedicals, Aurora, OH, USA), sodium bicarbonate ($NaHCO_3$, Fisher, Fair Lawn, NJ, USA), sodium hydroxide (NaOH, Fisher), and uranyl acetate dihydrate ($UO_2(CH_3COO)_2{\cdot}2H_2O$ (U as ^{238}U), International Bio-Analytical Industrial Inc., FL, USA). Humic acid (Leonardite Humic Acid Standard, St. Paul, MN, USA) was used to prepare HA stock solution and the ash part was removed by nylon membrane (0.45 μm pore size) filtration. The resultant HA stock solution contained 156 mg/L as total organic carbon (TOC).

2.2. Preparation of stabilized ZVI nanoparticles suspension

Stabilized ZVI nanoparticles suspensions were synthesized following an established method reported previously [16,17]. In brief, a stabilizer solution (100 mL of CMC or starch, 0.24% w/w) was purged with N_2 for 30 min in a flask to remove dissolved oxygen (DO). Then, freshly prepared $FeSO_4{\cdot}7H_2O$ solution (10 mL, Fe = 1.2 g/L) was added into the

flask and the mixture was further purged under N_2 for another 20 min to complete the formation of Fe^{2+}-CMC/starch complexes. Then, a borohydride solution (10 mL, 1.62 g/L) was injected into the mixture in 2 min under continuous vacuuming while being shaken at 250 rpm on a shaker. The BH_4^-/Fe^{2+} molar ratio was 2:1. The reactor was shaken for another 5 min, and then left still for 10 min. The resultant ZVI nanoparticles suspension contained 0.1 g/L as Fe^0 and 0.2% (w/w) of starch or CMC. Before use, the freshly synthesized ZVI nanoparticles slurry was purged with N_2 gas for 5 min to remove residual H_2 and to exhaust any unreacted $NaBH_4$ to eliminate their interference on U removal.

2.3. FTIR, and XPS analyses

Fourier transform infrared (FTIR) spectroscopy spectra were obtained for bare ZVI, CMC-ZVI, U-CMC-ZVI nanoparticles (uranium immobilized on CMC-ZVI nanoparticles), U-HA-CMC-ZVI nanoparticles (U treated in the presence of HA). To this end, ZVI nanoparticles were prepared (35 mg/L as Fe) and then reacted with 25 mg/L U(VI) for 1 day at a constant pH ~6.2. Upon equilibrium, the solids were collected in a N_2-filled glovebox then freeze-dried, and mixed with KBr to obtain pellets consisting of ~2 wt.% of the nanoparticles. Then the pellets were analyzed using a SHIMADZU IR spectrometer (model Prestige-21, Shimadzu Scientific Instruments, Columbia, MD, USA). For comparison, FTIR spectra for neat CMC/starch powder were also obtained in the same manner.

X-ray photoelectron spectroscopy (XPS) measurements were performed using a load-locked Kratos XSAM 800 surface analysis system equipped with a hemispherical energy analyzer. Again, the solid samples were collected in a N_2-filled glovebox then freeze-dried to prevent them from being oxidized. Detailed XPS settings are provided in Section S1 in Supplementary Materials, SM.

2.4. Effects of stabilizers and pH on U(VI) removal by stabilized ZVI nanoparticles

Bare ZVI, starch-ZVI and CMC-ZVI nanoparticles were synthesized and compared for U(VI) removal under otherwise identical conditions. The tests were initiated by adding 120 mL of a ZVI nanoparticles suspension (Fe° = 0.1 g/L with stabilizer = 0 or 0.2 wt.%) into 233 mL of a U(VI) solution (U = 38 mg/L, see Section S2 in SM for details about U solution preparation) and the mixture was transferred into 30 mL polycarbonate vials with nearly zero head space. The resultant experimental conditions were: initial U = 25 mg/L, Fe = 35 mg/L, buffer = 10 mM, and starch or CMC = 0.2 wt.%. The vials were agitated on a rotator at 60 rpm in an incubator at 22 ± 1 °C. At predetermined time intervals, the vials were sacrificially sampled under N_2 purging, and 10 mL of each sample was filtered through a cellulose acetate membrane (pore size = 50 nm, Merck Millipore Ltd. Germany) in a glovebox, and then the filtrates were acidified with HNO_3 (5 M) to pH ~2, and then analyzed for U remaining in the aqueous phase.

To probe pH effect, the kinetic tests were carried out at pH 5.0 − 9.0. A common buffer HAc/NaAc (10 mM) was used to keep pH at 5.0 or 6.0, whereas a Tris buffer (10 mM) was used at pH 7.0–9.0. Both buffers have been used in previous studies and no effects were found on ZVI reactivity [4,10,22]. Control tests with or without the buffers in this study confirmed the negligible effect of buffers on U(VI) removal. U(VI) adsorbed on the ZVI particles was determined via the bicarbonate extraction method (Section S3 in SM).

2.5. Soil deliverability test of bare and stabilized ZVI nanoparticles

To compare the soil deliverability of bare and stabilized ZVI nanoparticles, column tests were carried out to obtain the breakthrough curves of the nanoparticles. The soil treatment method and results are provided in Section S4 and Table S1 in SM, respectively. The column setup included a Harvard Apparatus PHD 2000 syringe pump (Plymouth Meeting, PA, USA), a Plexiglas column (inner diameter = 10 mm, length = 120 mm, Omnifit, Cambridge, UK), and a fraction collector (Eldex Laboratories, Napa, CA, USA). First, sandy soil (12 g) was added from the top into the column containing a nitrogen-purged background solution (0.84 mM NaCl and 0.16 mM $NaHCO_3$, pH 7.5) under constant patting with a plastic rod, resulting in a soil porosity of 0.34 and a bulk bed volume of 8.8 mL (bed height = 11.2 cm, unit pore volume = 2.99 mL, bed volume = 8.79 mL, Empty bed contact time = 29.9 min). Then, a suspension of bare ZVI, (starch-ZVI or CMC-ZVI nanoparticles) was pumped through the soil column in the down-flow mode at a flow rate of 0.04 or 0.2 mL/min. The effluent was collected by a fraction collector. The samples were then acidified using HCl (12 M) at 1:1 volume ration to completely dissolve ZVI, and then analyzed for total Fe (i.e., ZVI concentration in the effluent). To probe the hydrodynamic characteristics of the column system, tracer tests were conducted with a KBr solution (50 mg/L as Br^-) under identical operating conditions.

2.6. Effects of ligands on U(VI) immobilization

The U(VI) solution in the presence of HA or $NaHCO_3$ was prepared following the procedure described in Section S2 in SM. The kinetic tests were carried out following the same protocols as described in Section 2.4 under otherwise identical conditions with HA = 10 or 20 mg/L as TOC, $NaHCO_3$ = 1 mM or 5 mM, and $Ca(NO_3)_2$ = 1 mM.

2.7. Remobilization tests: effects of HA, bicarbonate and oxic conditions

Soluble U(VI) was first immobilized following the same kinetic test procedures and after equilibrium was reached, remobilization rates of U were tested by measuring the soluble U under various water chemistry conditions. First, the remobilization tests were conducted under anoxic conditions and in the presence or absence of HA or bicarbonate. To this end, 20 mL of N_2 purged DI water, or concentrated HA or HCO_3^- solutions were added into the suspensions, resulting in the following initial conditions: HA = 0, 10 or 20 mg/L as TOC, $NaHCO_3$ = 1 mM or 5 mM. Then the mixtures were transferred into 30 mL polycarbonate vials with zero head space and capped with Teflon-lined septa in a glove box filled with pure N_2. At predetermined time intervals, the vials were sacrificially sampled in the glove box. The samples were filtered to remove the nanoparticles and then filtrates were analyzed for soluble U. To test the effect of DO, the same remobilization experiments were also carried out under oxic conditions, with the bottles open to the air during the aging process.

2.8. Remobilization tests: effects of microbial activities

To test the effects of microbial activities on the stability of immobilized U, the remobilization experiments were also carried out in the presence a consortium of microorganisms. To this end, a slurry (~2 L) with mixed culture of anaerobic microbes and sediment was collected from a lake, Auburn, AL, USA (N32.588/W85.485). The slurry was stirred and cultivated under anaerobic conditions for 24 h. Then, the microbial suspension (10 mL) was inoculated into 1600 mL of the CMC-ZVI nanoparticles treated uranium suspension in a 2 L flask. For comparison, controls tests with a U(VI) solution (U = 35 mg/L) and DI water were also tested in parallel. A nutrition feed solution was prepared following the reported method [23], and 200 mL of the feed solution was initially added into each anaerobic reactor to initialize the culture. Starting Day 13 of the inoculation, the feed solution was added daily at 30 mL/day. Meanwhile, the suspensions were sampled (30 mL each time) and analyzed for total soluble U and the total bacteria number (TBN). TBN was estimated following the fluorochrome staining method [24].

2.9. Chemical analyses

Total U in solution was analyzed via an ICP-OES (Varian 710-ES, Palo Alto, CA, USA, detection limit = 0.08 mg/L) or, if concentration were below 1 mg/L, re-measured by a KPA (kinetic phosphorescence analyzer) (model KPA-11, Chemchek Instruments, Richland, WA, USA, detection limit = 1.0 μg/L). Total dissolved Fe was analyzed with a flame atomic absorption spectrometer (Varian SpectraAA 220FS, Varian, Canton, MA, USA). Solution pH, DO, and oxidation reduction potential (ORP) were measured using an Oakton benchtop 510 pH meter, a 700 DO meter and a 2700 ORP meter (Oakton, CA, USA), respectively. TOC was determined via a Tekmar Dohrmann Pheonix 8000 UV-Persulfate TOC analyzer (Mason, OH, USA) with a detection limit of 0.1 mg/L.

3. Results and discussion

3.1. Effects of stabilizers on ZVI nanoparticles and U(VI) immobilization

Fig. S1 in SM compares the TEM images of bare ZVI, starch-ZVI and CMC-ZVI nanoparticles. Apparently as shown in Fig S1a, ZVI formed bulky dendritic flocs in the absence of stabilizers. Introduction of stabilizers (starch or CMC = 0.2% w/w) could create discrete nanoparticles as shown in Fig S1b and 1c. Based on the TEM measurement, the average particle size for starch-ZVI nanoparticles is 63.7 ± 7.8 nm (standard deviation), compared to 31.2 ± 4.1 nm for CMC-ZVI nanoparticles.

Fig. S2 in SM presents removal efficiency of U(VI) by CMC-ZVI with CMC/Fe molar ratio range of 0 − 0.0248. For ZVI dosage of 25 mg/L, bare ZVI (CMC/Fe = 0) removed 86% of U(VI) after equilibrium, and application of CMC at a CMC/Fe ratio of 0.0124 (resultant CMC = 0.2% w/w) could slightly increase the removal efficiency to 87%. While further increasing the CMC/Fe ratio to 0.0186 and 0.0248, the removal efficiency dropped to 81% and 63%, respectively. While for a ZVI dosage of 35 mg/L, U(VI) was fully removed at CMC/Fe ratio ranged from 0 to 0.0124. Again, the removal efficiency decreased at elevated CMC concertation. Higher ratio can produce smaller sized ZVI nanoparticles. For example, at CMC/Fe ratio of 0.0062, nearly 94% of ZVI will aggregate forming particles larger than 3 μm. While further increasing the ratio to 0.0124 and 0.0248 will produce ZVI with mean hydrodynamic diameters of 18.6 nm and 15.3 nm [17]. The smaller size of ZVI can provide larger surface area and more reaction sites. While in this study, the smaller sized CMC-ZVI did not provide sound removal enhancement suggesting the gain of larger surface area did not lead to the higher reactivity. For the aspects of ZVI surface, the excessive accumulation of CMC will create a denser coating resulting in a blockage of reaction sites [25]. Considering both the removal efficiency and stabilization efficiency, 35 mg/L of ZVI with CMC/Fe ratio of 0.0124 (or resultant CMC = 0.2% w/w) was the optimal condition and adopted in this work.

Starch is a neutral poly-sugar, which stabilizes ZVI nanoparticles through steric hindrance. While CMC carries negatively charged carboxymethyl groups (pK_a = 4.3), which prevent the ZVI nanoparticles from aggregation through combined electrostatic and steric stabilization mechanism. As a result, CMC is a more effective stabilizer than starch, and indeed, the size of starch-ZVI nanoparticles were almost twice that of CMC-ZVI nanoparticles based on TEM measurements. Stabilizer molecules can either be adsorbed on the surface of nanoparticles or exist in the aqueous phase, thereby stabilizer may influence the interactions between ZVI and U(VI) differently. In terms of reactivity, organic stabilizers may affect the reaction of ZVI with various contaminants in a number of ways. First, the stabilizer coating can modify the surface properties of ZVI nanoparticles and influence the interactions with the target contaminants. For the case of starch, the sorption of the neutral starch layer may add a barrier that inhibits both mass transfer and contact between U(VI) and electron donor (ZVI); for CMC ZVI nanoparticles, the adsorbed CMC molecules became increasingly ionized with increasing pH (5.0–9.0), rendering a rather negative surface potential. On the other hand, the predominant U(VI) species may shift from positively charged species (e.g., UO_2^{2+}, $(UO_2)_3(OH)_5^+$, $(UO_2)_4(OH)_7^+$, $(UO_2)_2(OH)_2^{2+}$, and UO_2OH^+) to negatively charged

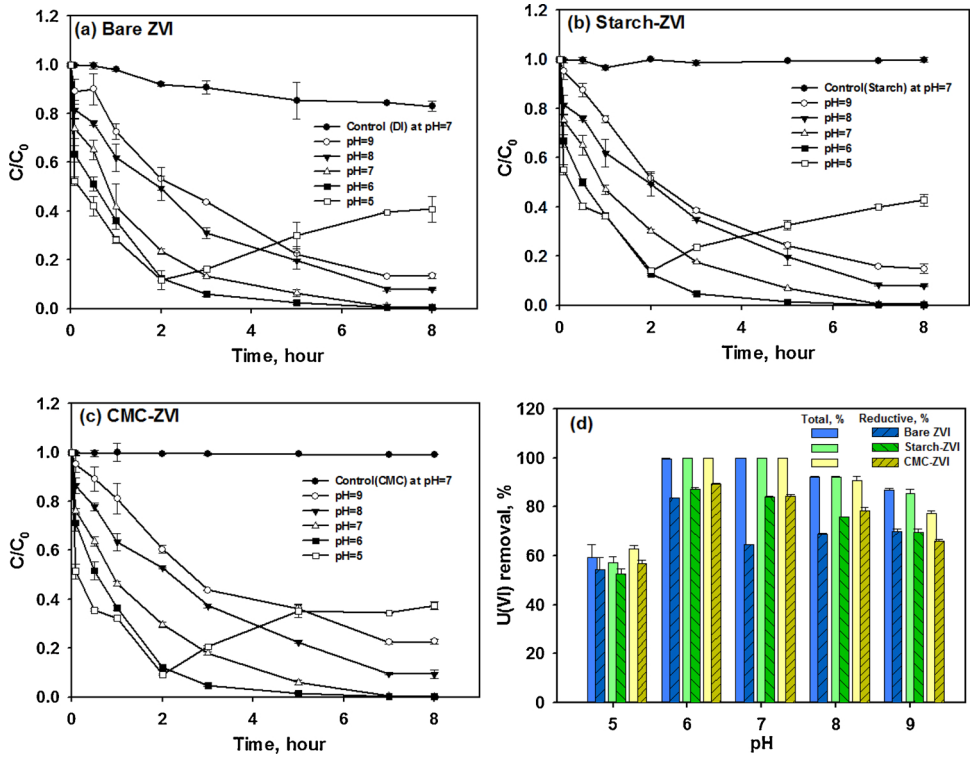

Fig. 1. U(VI) removal kinetics by: (a) Bare ZVI, (b) Starch-ZVI, (c) CMC-ZVI at different pH levels and (d) total or reductively removed U(VI). Conditions: initial U (VI) = 25 mg/L, ZVI = 35 mg/L for all cases, starch or CMC = 0.2% (w/w), pH were controlled at 5, 6, 7, 8 or 9.

ones ($(UO_2)_3(OH)_7^-$, $UO_2(OH)_3^-$, $UO_2(OH)_4^{2-}$) as pH increases (Details about U(VI) speciation can be found in Section S5 in SM) [26,27], thereby the negative coating of CMC-ZVI nanoparticles will repel the U (VI) resulting in a inhibition. Second, these organic polyelectrolytes may act as poly-dentate ligands and complex with chemicals such as heavy metals. In this case, such complexation effects may inhibit the reduction of U(VI) due to the increased barrier effect. Third, the organic stabilizers may compete the reaction sites with target contaminants thereby inhibiting the reaction between ZVI and contaminants. Fourth, the organic stabilizer (either as a surface coating or as a solute) may serve as a catalyst via shuttling electrons between ZVI nanoparticles and contaminants mediating the electron transfer. The overall effects of stabilizers depend on the balance of above four effects and both inhibition and acceleration of contaminant removal are possible, and apparently in this study, the inhibitive effect of stabilizer coating overweighed the positive effect from the reduced particle size. Thereby no significant enhancement was observed for stabilized ZVI nanoparticles than bare ZVI nanoparticles.

3.2. Effects of pH on U(VI) immobilization

Fig. 1a, 1b, and 1c show the kinetics of U(VI) removal at pH 5–9 via bare ZVI, starch-ZVI and CMC-ZVI nanoparticles, respectively. For all three types of ZVI nanoparticles, in pH range of 6–9, the U(VI) removal displayed a rapid initial (< 2 h) rate and then slowed down till equilibrium at ~7 h. While at pH 5, an even faster removal rate of U(VI) was observed for the first 2 h followed by a gradual release. As shown in Fig. 1d, the total U(VI) removal and reductively removed U(VI) were plotted as a function of pH for three types of ZVI nanoparticles. The overall U(VI) total removal efficiency increased from ~60% to > 99.6% as pH increased from 5 to 6 for all ZVI nanoparticles. Complete U(VI) removal remained at pH 7 then dropped at higher pH. Both bare ZVI nanoparticles and stabilized ZVI nanoparticles provided comparable total U(VI) removal at pH 5–8, while at pH 9, CMC-ZVI nanoparticles can only remove 77% of U(VI), which was lower than the efficiency of bare ZVI nanoparticles (86%) and starch-ZVI nanoparticles (85%). For the reductively removed U(VI), the removal efficiency peaked at pH 6 then dropped at higher pH level for both types of stabilized ZVI nanoparticles. While for bare ZVI nanoparticles, lowest reductive removal efficiency was observed at pH 7, at which level the reported minimum U(VI) solubility is only ~0.95 mg/L at pH 7.2 [28], suggesting the precipitation of schoepite ($UO_3{\cdot}H_2O$) could play an important role for total U(VI) removal. A slight drop of control for bare ZVI nanoparticles were observed (Fig. 1a) at pH 7, suggesting the formation of U(VI) precipitant. While for starch- and CMC-ZVI group (Fig. 1b and c), the control curves kept stable, again indicating the potential effects of organic matter on the apparent solubility of U(VI). Detailed discussion can be found in Section 3.4 and Section S5 in SM.

The removal kinetics data of ZVI nanoparticles can be interpreted using a pseudo-first-order rate model [29]:

$$\frac{d[U(VI)]}{dt} = -k_{obs}[U(VI)] = -k_{SA}a_s\rho_m[U(VI)] \quad (1)$$

where [U(VI)] is the U(VI) concentration (mg/L) in water at time t (h), k_{obs} is the observed pseudo-first-order rate constant (1/h), k_{SA} is the specific reaction rate constant based on surface area of the nanoparticles (L/(h m^2)), a_s is the specific surface area of the nanoparticles (m^2/g), and ρ_m is the mass concentration of the nanoparticles (g/L). Assuming ZVI nanoparticles are non-porous, the specific surface area (a_s) values can be calculated based on the diameters (d) obtained through TEM images following the equation [30]:

$$a_s = \frac{\text{Surface are}}{\text{Mass}} = \frac{\pi d^2}{\rho\frac{\pi}{6}d^3} = \frac{6}{\rho d} \quad (2)$$

where ρ is the density (7800 kg/m^3 for iron) of the solid particle. The size of starch-ZVI and CMC-ZVI can be obtained via TEM image, and calculated specific surface area is 12.1 and 24.7 m^2/g, respectively. To give a sound comparison, we took the measured BET surface area of 14.5 m^2/g for bare ZVI nanoparticles [30], since their sizes are not attainable from TEM images. Table 1 gives the fitted model parameters. Fairly good fitting was obtained for all three types of ZVI nanoparticles in pH range of 6–9. And again, the higher observed rate constant (k_{obs}) was observed at lower pH. At pH 6, the observed rate constant (k_{obs}) followed the order of CMC- > starch- > bare ZVI nanoparticles, while at pH 7–9 order changed to bare ≥ starch- > CMC-ZVI nanoparticles. Based on the k_{SA} values, the starch-ZVI nanoparticles offered the highest reactivity despite the CMC-ZVI nanoparticles possess two times larger specific surface area.

3.3. Soil deliverability of bare and stabilized ZVI nanoparticles

In addition to surface modification, another key merit of particle stabilization is to facilitate the delivery of ZVI nanoparticles into soil or deep aquifer for *in situ* remediation of target contaminants. The deliverability of all three types of ZVI nanoparticles were compared based on the breakthrough curves plotted in Fig. 2. The KBr tracer breakthrough occurred sharply at ~1 pore volume (PV) and reached the plateau at ~2 PV indicating the negligible dispersion effect under the experimental conditions. For stabilized ZVI nanoparticles, all breakthrough started within 1 PV and reached full breakthrough at ~7 PV. For CMC-ZVI nanoparticles, C/C_0 kept at constant of ~96% for a low flow rate of 0.2 mL/min. With a lower flow rate (0.04 mL/min), C/C_0 was ~86% and the 14% loss of ZVI nanoparticles could address to the filtration effect in packed column. The starch-ZVI nanoparticles can only yield a C/C_0 of ~ 81% under identical conditions, suggesting the deliverability of starch-ZVI was poorer than CMC-ZVI. In contrast, nearly all the bare ZVI nanoparticles were trapped on the top of soil column and no ZVI were detected after ~9 PV. The results prove the feasibility for delivering the stabilized ZVI nanoparticles into the target subsurface zone. For practical design, the ZVI nanoparticles can be delivered into the desired zone via controlling the injection pressure and delivered ZVI nanoparticles will be immobile when external pressure is removed [31]. Due to its higher soil deliverability, the CMC-ZVI nanoparticles was employed for further tests in this study.

3.4. Effects of ligands on the U(VI) immobilization by CMC-ZVI nanoparticles

Fig. 3 shows the removal of U(VI) by CMC-ZVI nanoparticles with the presence of HA and $NaHCO_3$ as typical groundwater ligands. This part aims to examine the feasibility of CMC-ZVI nanoparticles for

Table 1
Observed pseudo-first-order rate constants (k_{obs}) and fitted specific reaction rate constants (k_{SA}) for three types of ZVI at pH 6-9.

ZVI types/pH	k_{obs} (1/h)	k_{SA}(L/(h m^2))	R^2
Bare ZVI			
6.0	0.71	1.40	0.97
7.0	0.71	1.40	0.98
8.0	0.32	0.63	0.93
9.0	0.27	0.53	0.91
Starch-ZVI			
6.0	0.86	2.04	0.92
7.0	0.71	1.68	0.97
8.0	0.32	0.74	0.99
9.0	0.26	0.60	0.93
CMC-ZVI			
6.0	0.99	1.15	0.94
7.0	0.70	0.81	0.92
8.0	0.29	0.34	0.99
9.0	0.20	0.23	0.97

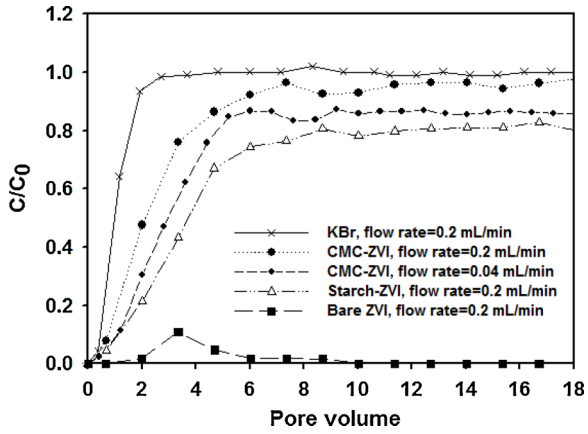

Fig. 2. Breakthrough curves of a KBr tracer, bare ZVI, starch-ZVI and CMC-ZVI nanoparticles through a sandy soil. Br- = 50 mg/L, ZVI = 35 mg/L for all three types, stabilizer = 0.2% w/w. C and C_0 are influent and effluent concentrations, respectively.

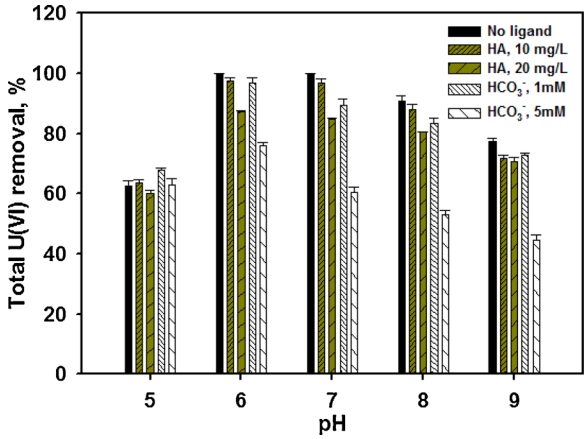

Fig. 3. Total U(VI) removal by CMC-ZVI nanoparticles with the presence of HA or $NaHCO_3$. Initial U(IV) = 25 mg/L, ZVI = 35 mg/L, HA = 10 or 20 mg/L as TOC, $NaHCO_3$ = 1 mM or 5 mM.

immobilizing the U-HA and U-CO_3^{2-} complex. The introduction of 10 mg/L of HA did not cause a significant retardation for U(VI) removal (in all the cases, the decreased U removal < 7%). While with doubled amount of HA added, the U(VI) removal efficiency was decreased more than 10% at pH 5–8, and 7% for at 9. Similarly, the addition of small amount of $NaHCO_3$ (1 mM) did not cause profound retardation of U(VI) removal (in all cases, the drop of removal efficiency was less than 8%). However, addition of Ca^{2+} (1 mM) can further decreased the U(VI) removal from 96.5% to 89.3% at pH 6. With elevated concentration of $NaHCO_3$ (5 mM), the inhibition effects were more profound, especially at pH higher than 6.

HA in the groundwater system can exist in both aqueous phase and be sorbed onto particle surface. The aqueous HA can predominantly form soluble binary UO_2HA(II) and ternary complex UO_2(OH)HA(I) in a pH range of 4.5–9 [32]. The addition of HA can significantly increase the mobility of U(VI) at anaerobic conditions and the strength of this solubilizing effect was found positively correlated with the hydrophobicity of organic matter [33,34]. The U(VI) solubility was enhanced with addition of HA (see Section S5 in SM). It is reported that the HA can chelate with the shell of ZVI nanoparticles through hydroxyl and carboxylic groups thereby forming a compact layer [35]. As demonstrated in the FTIR spectra (Fig. 5), the complex of U-HA was accumulated in the U-HA-CMC-ZVI nanoparticles sample and these sorbed HA can also pose several effects on ZVI nanoparticles reactivity. Firstly, the HA can compete with CMC for the site on ZVI surface thereby diminish the stabilizing effectiveness. It was observed that the addition of 20 mg/L of DOM increased the hydraulic diameter of CMC-ZVI nanoparticles from 222 nm to 295 nm [36]. Secondly, HA molecules on ZVI nanoparticles surface can form a mass transfer barrier and block the reaction sites. Inhibitory effects was observed for reductive degradation of chlorinated organics by ZVI nanoparticles, which was generally ascribed to competition for reactive sites between adsorbed HA and target contaminants [37]. Thirdly, the immobilized HA on ZVI nanoparticles surface can also serve as sorption sink for U(VI) thereby adsolubilizing U(VI). Sorption of U(VI) onto phyllite was observed to be highly dependent on the uptake of HA onto phyllite and more uptake of HA can lead to an enhanced sorption of U(VI) [38].

With the presence of $NaHCO_3$/Na_2CO_3 at pH > 6, the uranyl ion can complex with carbonate and form several types of complex ($UO_2(CO_3)_3^{4-}$, $UO_2(CO_3)_2^{2-}$, and $(UO_2)_2CO_3(OH)_3$- as shown in Fig. S7 and S8 in SM), which are more stable than soluble uranyl hydroxide. The negatively charged the uranyl complex will consequently repel the negatively charged CMC-ZVI nanoparticles thereby further limiting the surface contact. It was observed that rate-determining step for the overall U(VI) removal reaction by bare ZVI nanoparticles shifted from reduction to sorption after bicarbonate added [13]. Carbonate is believed to have stronger effects on ZVI nanoparticles corrosion than DOM [39]. The added bicarbonate can be sorbed onto ZVI nanoparticles surface and react as oxidant following the reaction [40]:

$$Fe^0+2H_2CO_{3(ads)} \leftrightarrow Fe^{2+} + H_2 + 2HCO^-_{3(ads)} \quad (3)$$

$$Fe^0+2HCO^-_{3(ads)} \leftrightarrow Fe^{2+} + H_2 + 2CO^{2-}_{3(ads)} \quad (4)$$

The precipitated carbonate can also coat on the iron surface thereby inhibit the further reaction [40,41]. The proposed overall reaction equation is expressed as [25,42]:

$$Fe^0+UO_2(CO_3)_3^{4-}+6H^+ \rightarrow UO_2+Fe^{2+}+3CO_2+3H_2O \quad (5)$$

According to Eqn. (5), the reduction of uranyl carbonate complex via ZVI nanoparticles is also thermodynamically favored at lower pH. The introduction of Ca^{2+} can further inhibit the U(VI) removal by ZVI, and the main reasons could be: a) Ca^{2+} can suppress the stability of ZVI nanoparticle suspension resulting in decreased stability and reactivity of stabilized nanoparticles [43]; b) Ca^{2+}, as a strong cation, can also compete with the uranyl oxycations for the reaction sites [44]; c) Ca^{2+} can form strong Ca-U-carbonate complexes ($CaUO_2(CO_3)_3^{2-}$ or $Ca_2UO_2(CO_3)_3$(aq)) hindering the removal of U(VI) [44,45].

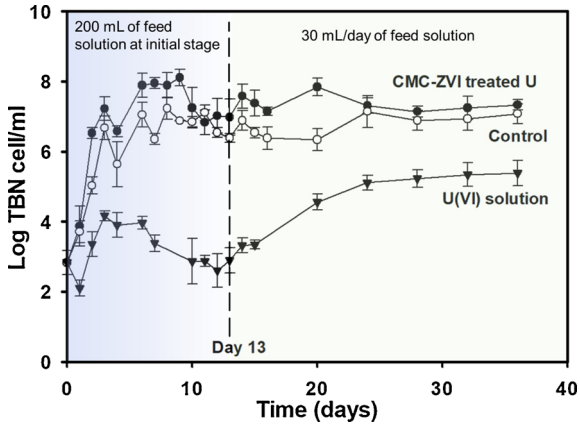

Fig. 4. Bacterial growth measured by total bacteria number (TBN) in CMC-ZVI treated uranium solution, U(VI) solution, and DI water as control. Experiential conditions: pH = 6.5-7.2, temperature = 21 ± 0.5 °C. At the beginning, 200 mL of the feed solution was added to initialize the culture. Starting Day 13, the feed solution was added daily at 30 mL/day.

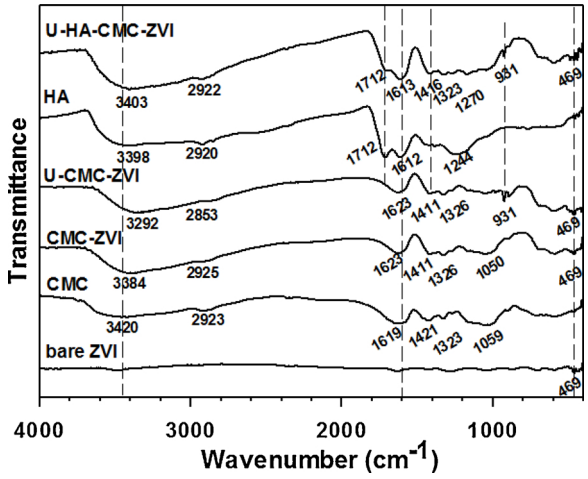

Fig. 5. FTIR spectra of bare ZVI, neat CMC powder, CMC-ZVI, spent CMC-ZVI, HA and CMC-ZVI reacted with HA-U.

3.5. Remobilization test: effects of anoxic and oxic conditions

The evolution of treated U(VI) in a buffered system with/without ligands during the 6-month remobilization test is tabulated in Table S2 in SM. The conditions were well controlled under anoxic, as pH ranged 6.7–7.2, DO < 1 mg/L and Fe release < 2.5% in all cases.The introduction of HA = 10 mg/L or CO_3^{2-} of 1 mM did not cause significant release of U(VI). While the addition of higher dose of HA or CO_3^{2-} lead to a dissolution of U(VI) up to 7.2 and 10.1% respectively after 6 months. Doubling the dosage of ZVI nanoparticles could effectively reduce the U(VI) release.

The ORP values are indicative of both the aggregation state and reactivity of ZVI nanoparticles. DOM is known to strongly influence the aggregation and electrochemical properties of ZVI nanoparticles thereby altering the ORP of the solution [46]. The interactions between HA and ZVI nanoparticles surfaces can impact the aggregation of ZVI nanoparticles. In addition, the sorbed DOM is expected to decline the reduction potential of structural Fe(II) sites, making them poorer reductants [41]. Thus, with the addition of HA, more pronounced rebound of ORP was observed. The introduced bicarbonate can react with the residual ZVI nanoparticles (as discussed in Section 3.4) and ORP increased as gradual passivation of the iron due to formation of authigenic precipitates (siderite and perhaps green rust) [39]. In summary, the reduced U can persistently exist under reducing conditions in a controlled pH range, while the sorbed U(VI) can be released when subjected to stronger ligands.

Table S3 in SM shows the remobilization of uranium treated with 35 and 70 mg/L of CMC-ZVI nanoparticles under anoxic and oxic conditions without buffers. Under anoxic conditions, there was no soluble U (VI) observed after 1 month for the case of U treated by 35 mg/L of CMC-ZVI nanoparticles. Yet further aging data (6 months) showed the U(VI) re-dissolved ~ 1.2%. Upon exposed to the air, the dissolution was rapid and nearly 55% of treated uranium was re-dissolved after 6 months and all the U(VI) was oxidized to U(VI). The doubled dosage of ZVI nanoparticles can only inhibit the partial U(VI) release, but evidently after 6-month aging, all the U(IV) was oxidized back to U(VI). Detailed discussion can be found the Section 3.7 for the mechanisms of remobilization.

3.6. Remobilization test: effects of bioconditions

Fig. 4 presents the bacterial growth quantified by TBN of each batch. The initial TBN for each batch was 670 ± 153 while after 1 day of cultivation, the TBN increased by a factor of 10.9 and 7.6 times respectively for CMC-ZVI and control, suggesting the robust bacterial activity in both reactors. While for the batch with U(VI) solution, a modest drop of TBN was observed indicating the inhibition of U(VI) for bio-activity. During day 2 to day 9, the TBN almost increased exponentially for CMC-ZVI and control groups, yet evidently the growth rate of U(VI) solution batch was much slower. The evolution of U during the tests was tabulated in Table S4 in SM.

Aqueous U(VI) is toxic to many microorganisms and its toxicity is directly linked to the concentration of $UO_2^{2+}$and UO_2OH^+ [20,21]. Apparently, for the case of U(VI) solution, the bioactivity is suppressed by the U(VI) solution in this study at first. Eventually, the survived bacteria were likely to display tolerance to U(VI) and start to grow after 2 weeks. The neutral pH (~7) may cause the precipitation of schoepite resulting in a low U(VI) aqueous concentration. After two weeks, the detected U(VI) concentration was 0.1 mg/L, e.g. far below the theoretical solubility (~0.95 mg/L). The bacteria cell walls or extracellular polymeric substances can both contribute to the U(VI) sorption through complexation [19,47,48]. In addition, as bacteria grew the ORP became negative, which can also decrease the bioavailability of U(VI) [20].

For the case of CMC-ZVI nanoparticles treated U, the enhanced initial bioactivity can mainly due to: a) the low ORP created by ZVI nanoparticles is more favorable for anaerobic biological activity [49]; b) the CMC coating (~0.7 g/L) can also act as an energy source for the bacteria to stimulate microbial activity [18]. In addition, the CMC modification can lower the biotoxicity of ZVI nanoparticles to bacteria [50]. Thus, this result suggested that the exhausted ZVI nanoparticles did not display any toxic effect to bacteria.

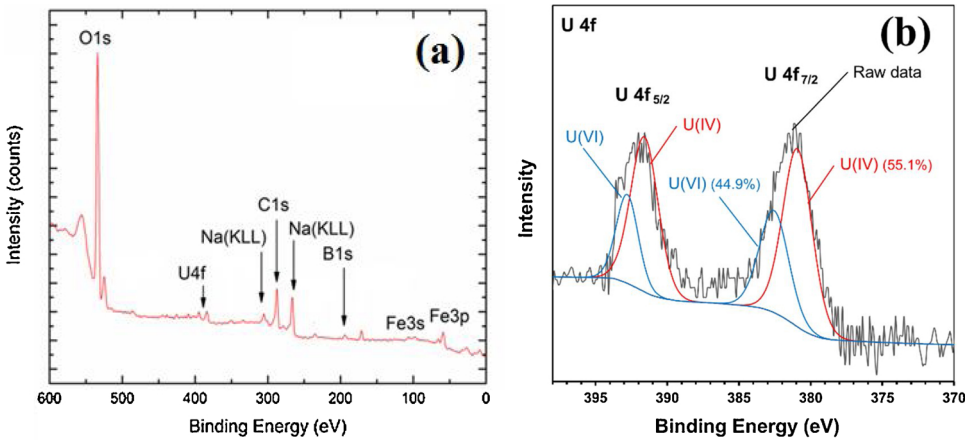

Fig. 6. XPS survey spectrum for (a) CMC-ZVI upon reaction with U(VI), and (b) high resolution spectrum over the U4f7/2 peak.

3.7. Analysis of ZVI before/after reactions and reaction mechanisms

Fig. 5 presents the FTIR spectra of bare ZVI, CMC, CMC-ZVI nanoparticles, HA and CMC-ZVI reacted with U-bearing HA. For bare ZVI nanoparticles, the peak at 469 cm^{-1} corresponds to the Fe-O stretch of Fe_2O_3 [51,52]. There was no discernable peak in the wavenumber range of 1000 − 4000 cm^{-1}, reflecting the absence of any organic compounds. In contrast, six strong peaks were identified for CMC-ZVI nanoparticles at the wavenumbers of 3384, 2925, 1623, 1411, 1326 and 1050 cm^{-1}. For CMC, the peaks at 1619, 1421 and 1059 cm^{-1} represent the asymmetric and symmetric vibrations of COO- groups and C−O stretching, respectively. Compared to CMC, the −OH stretching band for CMC-ZVI shifted from 3420 to 3384 cm^{-1}, which can be attributed to the enhanced intermolecular hydrogen bonding between CMC and ZVI nanoparticles [17]. Furthermore, the wavenumber separation (Δ) between the asymmetric ν_{as} (COO-) (1623 cm^{-1}) and symmetric ν_s (COO-) (1411 cm^{-1}) stretches of or CMC-ZVI was determined to be 212 cm^{-1}, suggesting the binding between CMC and ZVI nanoparticles is governed by monodentate chelating interactions [17]. Upon reaction with U(VI), the −OH stretch vibration for CMC-ZVI shifted from 3384 to 3292 cm^{-1}. A new band occurred at 931 cm^{-1}, which is attributed to the asymmetric stretching vibration of UO^{2+} [53], suggesting the existence of adsorbed U(VI) on the CMC-ZVI nanoparticles surface. Moreover, the peak intensity in range of 400 − 500 cm^{-1} decreased, indicating weakly bonded oxygen with uranium due to the formation of UO_2CMC complex via bidentate binding [54]. For neat HA, four peaks were observed at 3398, 1712, 1612 and 1244 cm^{-1}. The peak at 3398 cm^{-1} indicates the abundance of −OH groups. After the reaction of U-HA with CMC-ZVI nanoparticles, the intensity of the peak at 1712 cm^{-1} decreased due to the partial conversion of the COOH to COO- groups due to binding of U with HA [53]. In addition, the −OH band for the U-HA laden CMC-ZVI nanoparticles shifted from 3398 to 3403 cm^{-1}, and the Δ was decreased from 212 cm^{-1} for CMC-ZVI to 197 cm^{-1} suggesting the formation of U-HA complexes on the CMC-ZVI nanoparticles surface. Therefore, HA and CMC may compete for complexing with aqueous U.

Fig. 6a shows the XPS spectra for uranium laden CMC-ZVI nanoparticles. The surface is largely composed of C, O, and Fe with a small amount of U (~ 0.2 wt.%) and trace amounts of other elements (Na, and B from $NaBH_4$). Fig. 6b shows high resolution photoemission scans over the $U4f_{7/2}$ (at ca. 380.8 eV) and $U4f_{5/2}$ (391.6 eV) spin states for the specimen. In each case of U4f, the broad feature can be de-convoluted into two sub-peaks suggesting variable oxidation states are present [55]. The relative percentiles of U(VI) and U(IV) were determined based on the $U4f_{7/2}$ separated peaks at 382.8 eV and 381.2 eV (Fig. 6b), respectively [56–58]. According to the peak areas, U(VI) and U(IV) accounted for 44.9% and 55.1% of total U, respectively. The results again confirmed the co-existence of both U(VI) and U(IV) on the surface of the spent CMC-ZVI, suggesting that both reduction and sorption contribute to the removal of U by ZVI. It is also noteworthy that the ratio of U(VI)/U(IV) was different from the results based on bicarbonate extraction method. This could be due to the partial oxidation of sample during XPS measurement or that XPS method can only provide the elemental results on the sample surface [45]. Moreover, another study revealed that > 80% of U is accumulated in the shell of ZVI nanoparticles at the first stage of reaction (1 h) based on scanning transmission electron microscopy [59], thus, it was also possible that more U(VI) was enriched in the surface in our work.

Reaction mechanisms: Generally, four types of possible mechanisms for U(VI) removal under anoxic conditions have been proposed (Fig. 7) [4,60]:

a) Precipitation:

$$UO_2^{2+} + 2OH^- + 2H_2O \leftrightarrow UO_3 \cdot 3H_2O\,(s) \quad (6)$$

b) Sorption:

$$UO_2^{2+} + 2 > Fe\text{-}OH \leftrightarrow [(>Fe\text{-}O)_2UO_2]_{ads} + 2H^+ \quad (7)$$

c) Fe(0) reduction:

$$Fe^0 + 1.5UO_2^{2+} + 6H^+ \rightarrow Fe^{3+} + 1.5U^{4+} + 3H_2O \quad E_0 = +0.17V \quad (8)$$

d) Structural Fe(II) reduction

$$UO_2^{2+} + 2Fe^{2+}_{structural} + 4H^+ \rightarrow U^{4+} + 2Fe^{3+}_{structural} + 2H_2O \quad (9)$$

Among the above four mechanisms, the first two are reversible while the rest two of them are irreversible. The U(VI) removed via precipitation and sorption are extractable using bicarbonate extraction method and these U(VI) can easily release. The precipitation of schoepite ($UO_3 \cdot 2H_2O$) is most significant at pH ~7.2 (detailed discussion can be found in Section S5 in SM). Thereby at pH 7 for bare ZVI nanoparticles, the precipitation of schoepite will inhibit the contact between ZVI nanoparticles and U(VI), resulting in a lowered reductive removal and the total removal was partially due to the precipitant (as shown in Fig. 1d). The sorption of U(VI) onto ZVI surface was mainly through proton exchanges (Eqn. 7) [60]. Previous reports also demonstrated that aged/exhausted ZVI nanoparticles shell may contain lepidocrocite, magnetite, goetithe and maghemite [61] and the

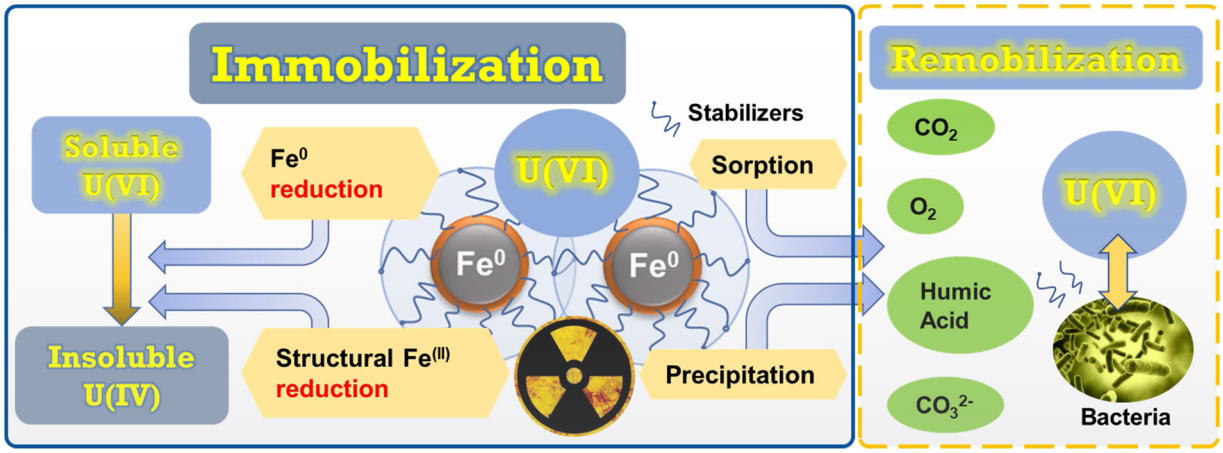

Fig. 7. Schematic representation of reaction mechanisms for U(VI) immobilization by CMC-ZVI and remobilization of U(VI).

hydroxyl groups on oxide layers can also adsorb U(VI) per proton exchanges. It is reported the sorption of U(VI) by magnetite peaked at pH ~6−8 [62,63]. In present work at pH 6–8, it is evident that the sorption and surface precipitation of U(VI) onto shell of ZVI nanoparticles also contributed to the total U(VI) removal (Fig. 1d).

For reduction approach, the reported E° for U(VI) reduction in aqueous phase is 0.327 V (Eqn. (10)), thus both Fe(0) (E_0 = -0.44 V) and structural Fe(II) (-0.65 V < E_0 < -0.34 V) are strong reducing agents capable of reducing U(VI) to U(IV). Previous study also reported that reduction is the major driving force for the total U(VI) removal [4,13,60,64–66]. And the reduced U(IV) will further precipitated as UO_2 (Eqn. (11)).

$$UO_2^{2+} + 2e^- + 4H^+ \rightarrow U^{4+} + 2H_2O \quad E^0 = +0.327V \tag{10}$$

$$U^{4+} + 2H_2O = UO^2(s) + 4H^+ \log K_{sp} = 4.832 \tag{11}$$

According to Eqns. (8) and (9), the reductive removal of U(VI) is thermodynamically more favorable in acidic solution, therefore higher efficiency of U(VI) reductive removal was observed at lower pH in the pH 6–9 for stabilized ZVI nanoparticles. Previous work also reported same trend for U(VI) removal by bare ZVI nanoparticles at pH 7–9 [13]. At alkaline pH, iron hydroxide shell on ZVI nanoparticles can impede the electro flow between ZVI nanoparticles and U(VI) resulting in an inhibited reduction. In addition, the more negative surface potential and stronger competition from hydroxyl anions at higher pH renders an unfavorable surface environment between CMC-ZVI nanoparticles and U(VI).

The anoxic corrosion of ZVI nanoparticles is also pH-dependent and follows the reaction [67]:

$$2H_2O + Fe^0 \rightarrow Fe^{2+} + 2OH^- + H_2 \tag{12}$$

From pH 8.2 to 6.0, the corrosion rate of CMC-ZVI nanoparticles increased by ~31.4 times and 11.5 times for trichloroethene reduction rate suggesting a strong correlation between iron corrosion and degradation of target contaminant [25]. Same trend was observed for pH 6–9 in this study, while at pH 5, the corrosion reaction can competitively consume the ZVI nanoparticles reactivity resulting in a suppressed U(VI) removal and a gradual release after 2 h. Similar re-dissolution was reported for U(VI) removal by bare ZVI nanoparticles after 1 h-reaction at pH 3–5, and extensive release of Fe was also evident (~89% at pH 3 and 4, and ~51% at pH 5) [4]. The destruction of ZVI nanoparticles structure is also evidenced by the Fe release in this study as shown in Fig. S11 in SM. Evidently, more Fe dissolution was observed at lower pH levels (~72%, 21% and 5% at pH 5, 6 and 7, respectively, < 1% dissolution at pH 8–9). A recent study revealed that > 80% of U is accumulated in the shell of ZVI nanoparticles after 1 h, while after equilibrium (24 h), 38% of total U is safely encapsulated in the ZVI nanoparticles core [59]. Thus, at pH 5 in present work, U(VI) in the shell can be released when the ZVI nanoparticles is rapidly and corrosively reacted within the first 2 h. The dissolution of Fe at acidic pH can also lead to the core depletion of ZVI nanoparticles resulting in rapid exhaustion of reduction potential from both ZVI nanoparticles and structural Fe(II) [68]. Therefore, the U(VI) removed at pH 5 is mainly through reductively precipitate other than sorption (Fig. 1d).

According to Eqn. (12), under anoxic conditions, the corrosion of ZVI nanoparticles can increase the solution pH. While under the oxic condition for the remobilization test, the intrusion of O_2 was evidenced in redound of DO after 1 day and a rapid ORP increase occurred concurrently since the DO can facilitate the ZVI nanoparticles oxidative corrosion per [42]:

$$2Fe^0 + 4H^+ + O_2 \rightarrow 2Fe^{2+} + 2H_2O \tag{13}$$

$$2Fe^{2+} + 2H^+ + 0.5O_2 \rightarrow 2Fe^{3+} + H_2O \tag{14}$$

According to Eqn. (13) and (14), the residual ZVI nanoparticles can further consume H^+ thus the accompanying pH increased at day 1 was primarily addressed to the reactions between ZVI nanoparticles and DO. In addition, the ingress of atmospheric CO_2 is also responsible for U(VI) release. The carbonate complex can be easily formed through [69]:

$$UO_2^{2+} + 2HCO_3^- \rightarrow UO_2(CO_3)_2^{2-} + 2H^+ \tag{15}$$

$$UO_2(CO_3)_2^{2-} + HCO_3^- \rightarrow UO_2(CO_3)_3^{4-} + H^+ \tag{16}$$

$$UO_2^{2+} + 2HCO_3^- + CO_3^{2-} \rightarrow UO_2(CO_3)_3^{4-} + 2H^+ \tag{17}$$

The uranyl complex on aged ZVI nanoparticles surface can react with H_2CO_3 following [25,42]:

$$(>FeOH)_2UO_2CO_{3(s)}^- + 2H_2CO_{3(aq)} \rightarrow 2(>FeOH^{0.5-})_{(s)} + UO_2CO_3^{4-}(aq) + 4H^+ \tag{18}$$

All these reactions (Eqn. (15)–(18)) can generate H^+, thereby a drop of pH (Table S3) was observed after 1 day when the treated U was subjected to air. The reduced form of U is also susceptible for carbonate leaching with the presence of O_2 [70]:

$$UO_{2(s)} + 3CO_3^{2-} + O_2 \rightarrow UO_2(CO_3)_3^{4-}$$

Therefor after exposed to air, the U(IV) is gradually oxidized to U (VI) and then released as carbonate complex. Eventually after 6 months, the remained U(VI) seemed still be trapped in the exhausted ZVI nanoparticles and can be extracted by carbonate. In summary, the overall gradual release of U under oxic condition is ascribed to the ingress of atmospheric oxygen and CO_2, and the reformation of carbonate complexes. Thus, under typical groundwater conditions, the reduced U(IV) can be safely immobilized and only U(VI) can be extracted by natural ligands. Moreover, the addition of stabilizers may prevent bacteria cell from being invaded by nanoparticles and stabilizers can serve as potential energy source for bacteria.

4. Conclusions

The experimental results highlight the potential use of ZVI nanoparticles in mitigate the U mobility and the summarized conclusions are:

1) In the pH range of 6–9, the lower pH enhanced the U(VI) reduction resulting in a faster removal kinetics and higher removal efficiency, yet at pH 5, the acidic corrosion of ZVI nanoparticles decreased U (VI) removal efficiency and caused a gradual release of U(VI);
2) CMC-ZVI nanoparticles presented better deliverability than starch-ZVI nanoparticles, and bare ZVI nanoparticles was almost trapped in the soil column;
3) The presence of low concentrations of HA (10 mg/L) and bicarbonate (1 mM) did not cause significant inhibitive effect while the higher dosage of ligands cause more profound inhibition of U(VI) removal;
4) Under anoxic conditions, no re-dissolution of treated U was detected in a well-controlled condition and the strong ligands can only desorb the extractable U(VI);
5) Yet upon to air, the treated U will be gradually oxidized and remobilized due to the ingress of atmospheric O_2 and CO_2;
6) CMC-ZVI nanoparticles treated U had almost no inhibition for the natural bacteria activity, suggesting the CMC-ZVI nanoparticles technology can effectively reduce the bio-toxicity of U(VI).

Declaration of Competing Interest

The authors declare that they have no known competing financial interests or personal relationships that could have appeared to influence the work reported in this paper.

CRediT authorship contribution statement

Xiao Zhao: Conceptualization, Investigation, Methodology, Software, Visualization, Writing - original draft. **Wen Liu:** Methodology, Resources, Visualization, Writing - review & editing. **Zhengqing Cai:** Resources, Investigation, Validation. **Jie Fu:** Resources, Methodology, Software. **Jun Duan:** Resources, Validation. **Dongye Zhao:** Conceptualization, Writing - review & editing, Supervision, Funding acquisition. **Michael Bozack:** Software, Visualization. **Yucheng Feng:** Methodology, Resources.

Acknowledgements

This work is partially supported by the National Natural Science Foundation of China (51809267, 41072265, 41230638 and 40810152) and an Auburn University VPR's IGP. Dr. Xiao Zhao is also grateful for the support by China Agricultural University Startup Fund (2020RC034).

Appendix A. Supplementary data

Supplementary material related to this article can be found, in the online version, at doi:https://doi.org/10.1016/j.colsurfa.2020.125315.

References

[1] M. Gavrilescu, L.V. Pavel, I. Cretescu, Characterization and remediation of soils contaminated with uranium, J. Hazard. Mater. 163 (2009) 475–510.
[2] R.G. Riley, J. Zachara, Chemical Contaminants on DOE Lands and Selection of Contaminant Mixtures for Subsurface Science Research, Pacific Northwest Lab., Richland, WA (United States), 1992.
[3] USEPA, National Primary Drinking Water Regulations, Radionuclides; Final Rule, 2003.
[4] O. Riba, T.B. Scott, K. Vala Ragnarsdottir, G.C. Allen, Reaction mechanism of uranyl in the presence of zero-valent iron nanoparticles, Geochim. Cosmochim. Ac. 72 (2008) 4047–4057.
[5] L. Xu, D. Zhang, F. Ma, J. Zhang, A. Khayambashi, Y. Cai, L. Chen, C. Xiao, S. Wang, Nano-MOF+ technique for efficient uranyl remediation, ACS Appl. Mater. Inter. 11 (2019) 21619–21626.
[6] N.A. Wall, G.R. Choppin, Humic acids coagulation: influence of divalent cations, Appl. Geochem. 18 (2003) 1573–1582.
[7] E.J. O'Loughlin, S.D. Kelly, R.E. Cook, R. Csencsits, K.M. Kemner, Reduction of uranium(VI) by mixed iron(II)/iron(III) hydroxide (green rust): formation of UO_2 nanoparticles, Environ. Sci. Technol. 37 (2003) 721–727.
[8] L.N. Moyes, R.H. Parkman, J.M. Charnock, D.J. Vaughan, F.R. Livens, C.R. Hughes, A. Braithwaite, Uranium uptake from aqueous solution by interaction with goethite, lepidocrocite, muscovite, and mackinawite: an X-ray absorption spectroscopy study, Environ. Sci. Technol. 34 (2000) 1062–1068.
[9] B. Hua, B. Deng, Reductive immobilization of uranium(VI) by amorphous iron sulfide, Environ. Sci. Technol. 42 (2008) 8703–8708.
[10] B. Hua, H. Xu, J. Terry, B. Deng, Kinetics of uranium(VI) reduction by hydrogen sulfide in anoxic aqueous systems, Environ. Sci. Technol. 40 (2006) 4666–4671.
[11] P. Wersin, M.F. Hochella, P. Persson, G. Redden, J.O. Leckie, D.W. Harris, Interaction between aqueous uranium(VI) and sulfide minerals: spectroscopic evidence for sorption and reduction, Geochim. Cosmochim. Ac. 58 (1994) 2829–2843.
[12] D.R. Lovley, E.E. Roden, E. Phillips, J. Woodward, Enzymatic iron and uranium reduction by sulfate-reducing bacteria, Mar. Geol. 113 (1993) 41–53.
[13] S. Yan, B. Hua, Z. Bao, J. Yang, C. Liu, B. Deng, Uranium(VI) removal by nanoscale zerovalent iron in anoxic batch systems, Environ. Sci. Technol. 44 (2010) 7783–7789.
[14] X. Zhao, W. Liu, Z. Cai, B. Han, T. Qian, D. Zhao, An overview of preparation and applications of stabilized zero-valent iron nanoparticles for soil and groundwater remediation, Water Res. 100 (2016) 245–266.
[15] B. Gu, L. Liang, M. Dickey, X. Yin, S. Dai, Reductive precipitation of uranium(VI) by zero-valent iron, Environ. Sci. Technol. 32 (1998) 3366–3373.
[16] F. He, D. Zhao, Preparation and characterization of a new class of starch-stabilized bimetallic nanoparticles for degradation of chlorinated hydrocarbons in water, Environ. Sci. Technol. 39 (2005) 3314–3320.
[17] F. He, D. Zhao, J. Liu, C.B. Roberts, Stabilization of Fe-Pd nanoparticles with sodium carboxymethyl cellulose for enhanced transport and dechlorination of trichloroethylene in soil and groundwater, Ind. Eng. Chem. Res. 46 (2007) 29–34.
[18] J. Zhou, Y. Deng, F. Luo, Z. He, Q. Tu, X. Zhi, Functional molecular ecological networks, mBio 1 (2010) e00169–00110.
[19] M.L. Merroun, S. Selenska-Pobell, Bacterial interactions with uranium: an environmental perspective, J. Contam. Hydrol. 102 (2008) 285–295.
[20] K.M. Belli, T.J. DiChristina, P. Van Cappellen, M. Taillefert, Effects of aqueous uranyl speciation on the kinetics of microbial uranium reduction, Geochim. Cosmochim. Ac. 157 (2015) 109–124.
[21] A. Tapia-Rodríguez, A. Luna-Velasco, J.A. Field, R. Sierra-Alvarez, Toxicity of uranium to microbial communities in anaerobic biofilms, Water Air Soil Pollut. Focus. 223 (2012) 3859–3868.
[22] F.Y.C. Huang, P.V. Brady, E.R. Lindgren, P. Guerra, Biodegradation of uranium – citrate complexes: implications for extraction of uranium from soils, Environ. Sci. Technol. 32 (1998) 379–382.
[23] Z. He, S.D. Minteer, L.T. Angenent, Electricity generation from artificial wastewater using an upflow microbial fuel cell, Environ. Sci. Technol. 39 (2005) 5262–5267.
[24] R. Kepner, J.R. Pratt, Use of fluorochromes for direct enumeration of total bacteria in environmental samples: past and present, Microbiol. Rev. 58 (1994) 603–615.
[25] D.M. Sherman, C.L. Peacock, C.G. Hubbard, Surface complexation of U(VI) on goethite (α-FeOOH), Geochim. Cosmochim. Ac. 72 (2008) 298–310.
[26] S.P. Hyun, J.A. Davis, K. Sun, K.F. Hayes, Uranium (VI) reduction by iron (II) monosulfide mackinawite, Environ. Sci. Technol. 46 (2012) 3369–3376.
[27] M.E. Kirby, J.S. Watson, J. Najorka, J.P.L. Kenney, S. Krevor, D.J. Weiss, Experimental study of pH effect on uranium (U^{VI}) particle formation and transport through quartz sand in alkaline 0.1 M sodium chloride solutions, Colloids Surf. A 592 (2020) 124375.
[28] C. Noubactep, G. Meinrath, P. Dietrich, B. Merkel, Mitigating uranium in groundwater: prospects and limitations, Environ. Sci. Technol. 37 (2003) 4304–4308.
[29] T.L. Johnson, M.M. Scherer, P.G. Tratnyek, Kinetics of halogenated organic compound degradation by iron metal, Environ. Sci. Technol. 30 (1996) 2634–2640.
[30] Y.-P. Sun, X.-q. Li, J. Cao, W.-X. Zhang, H.P. Wang, Characterization of zero-valent iron nanoparticles, Adv. Colloid Interface Sci. 120 (2006) 47–56.
[31] F. He, M. Zhang, T. Qian, D. Zhao, Transport of carboxymethyl cellulose stabilized iron nanoparticles in porous media: column experiments and modeling, J. Colloid Interface Sci. 334 (2009) 96–102.
[32] A. Křepelová, S. Sachs, G. Bernhard, Uranium(VI) sorption onto kaolinite in the presence and absence of humic acid, Radiochim. Acta 94 (2006) 825–833.
[33] W. Luo, B. Gu, Dissolution and mobilization of uranium in a reduced sediment by natural humic substances under anaerobic conditions, Environ. Sci. Technol. 43 (2008) 152–156.
[34] Y. Yang, J.E. Saiers, N. Xu, S.G. Minasian, T. Tyliszczak, S.A. Kozimor, D.K. Shuh, M.O. Barnett, Impact of natural organic matter on uranium transport through saturated geologic materials: from molecular to column scale, Environ. Sci. Technol. 46 (2012) 5931–5938.
[35] A.B. Giasuddin, S.R. Kanel, H. Choi, Adsorption of humic acid onto nanoscale zerovalent iron and its effect on arsenic removal, Environ. Sci. Technol. 41 (2007) 2022–2027.
[36] M. Zhang, F. He, D. Zhao, X. Hao, Degradation of soil-sorbed trichloroethylene by stabilized zero valent iron nanoparticles: effects of sorption, surfactants, and natural organic matter, Water Res. 45 (2011) 2401–2414.
[37] P.G. Tratnyek, M.M. Scherer, B. Deng, S. Hu, Effects of natural organic matter, anthropogenic surfactants, and model quinones on the reduction of contaminants by zero-valent iron, Water Res. 35 (2001) 4435–4443.
[38] K. Schmeide, S. Pompe, M. Bubner, K. Heise, G. Bernhard, H. Nitsche, Uranium(VI) sorption onto phyllite and selected minerals in the presence of humic acid, Radiochim. Acta 88 (2000) 723.
[39] J.T. Nurmi, P.G. Tratnyek, Electrochemical studies of packed iron powder electrodes: effects of common constituents of natural waters on corrosion potential, Corros. Sci. 50 (2008) 144–154.
[40] A. Agrawal, W.J. Ferguson, B.O. Gardner, J.A. Christ, J.Z. Bandstra, P.G. Tratnyek, Effects of carbonate species on the kinetics of dechlorination of 1,1,1-trichloroethane by zero-valent iron, Environ. Sci. Technol. 36 (2002) 4326–4333.
[41] J. Klausen, P.J. Vikesland, T. Kohn, D.R. Burris, W.P. Ball, A.L. Roberts, Longevity of granular iron in groundwater treatment processes: solution composition effects on reduction of organohalides and nitroaromatic compounds, Environ. Sci. Technol. 37 (2003) 1208–1218.
[42] R. Crane, M. Dickinson, I. Popescu, T. Scott, Magnetite and zero-valent iron nanoparticles for the remediation of uranium contaminated environmental water, Water Res. 45 (2011) 2931–2942.
[43] J. Duan, H. Ji, X. Zhao, S. Tian, X. Liu, W. Liu, D. Zhao, Immobilization of U(VI) by stabilized iron sulfide nanoparticles: water chemistry effects, mechanisms, and long-term stability, Chem. Eng. J. 393 (2020) 124692.
[44] W. Liu, X. Zhao, T. Wang, D. Zhao, J. Ni, Adsorption of U(VI) by multilayer titanate nanotubes: effects of inorganic cations, carbonate and natural organic matter, Chem. Eng. J. 286 (2016) 427–435.
[45] G. Bernhard, G. Geipel, T. Reich, V. Brendler, S. Amayri, H. Nitsche, Uranyl(VI) carbonate complex formation: validation of the $Ca_2UO_2(CO_3)_{(3)}$(aq.) species, Radiochim. Acta 89 (2001) 511–518.
[46] Z. Shi, J.T. Nurmi, P.G. Tratnyek, Effects of nano zero-valent iron on oxidation – reduction potential, Environ. Sci. Technol. 45 (2011) 1586–1592.
[47] B. Cao, B. Ahmed, D.W. Kennedy, Z. Wang, L. Shi, M.J. Marshall, J.K. Fredrickson, N.G. Isern, P.D. Majors, H. Beyenal, Contribution of extracellular polymeric substances from *Shewanella sp.* HRCR-1 biofilms to U(VI) immobilization, Environ. Sci. Technol. 45 (2011) 5483–5490.
[48] C. Ding, W. Cheng, Y. Sun, X. Wang, Effects of Bacillus subtilis on the reduction of U (VI) by nano-Fe°, Geochim. Cosmochim. Ac. 165 (2015) 86–107.
[49] Y. Feng, Y. Zhang, X. Quan, S. Chen, Enhanced anaerobic digestion of waste activated sludge digestion by the addition of zero valent iron, Water Res. 52 (2014) 242–250.
[50] H. Dong, Y. Xie, G. Zeng, L. Tang, J. Liang, Q. He, F. Zhao, Y. Zeng, Y. Wu, The dual effects of carboxymethyl cellulose on the colloidal stability and toxicity of nanoscale zero-valent iron, Chemosphere 144 (2016) 1682–1689.
[51] X. Zhang, S. Lin, Z. Chen, M. Megharaj, R. Naidu, Kaolinite-supported nanoscale zero-valent iron for removal of Pb^{2+} from aqueous solution: reactivity,

characterization and mechanism, Water Res. 45 (2011) 3481–3488.
[52] H. Ji, Y. Zhu, W. Liu, M.J. Bozack, T. Qian, D. Zhao, Sequestration of pertechnetate using carboxymethyl cellulose stabilized FeS nanoparticles: effectiveness and mechanisms, Colloids Surf. A 561 (2019) 373–380.
[53] K. Schmeide, S. Sachs, M. Bubner, T. Reich, K.H. Heise, G. Bernhard, Interaction of uranium(VI) with various modified and unmodified natural and synthetic humic substances studied by EXAFS and FTIR spectroscopy, Inorg. Chim. Acta 351 (2003) 133–140.
[54] P. Filip, D. Humelnicu, I. Humelnicu, T.B. Scott, R.A. Crane, Removal of uranium (VI) from aqueous systems by nanoscale zero-valent iron particles suspended in carboxy-methyl cellulose, J. Nucl. Mater. 443 (2013) 250–255.
[55] E.S. Ilton, P.S. Bagus, XPS determination of uranium oxidation states, Surf. Interface Anal. 43 (2011) 1549–1560.
[56] S. Tsarev, R.N. Collins, A. Fahy, T.D. Waite, Reduced uranium phases produced from anaerobic reaction with nanoscale zerovalent Iron, Environ. Sci. Technol. 50 (2016) 2595–2601.
[57] K. Yuan, E.S. Ilton, M.R. Antonio, Z. Li, P.J. Cook, U. Becker, Electrochemical and spectroscopic evidence on the one-electron reduction of U(VI) to U(V) on magnetite, Environ. Sci. Technol. 49 (2015) 6206–6213.
[58] D.D. Boland, R.N. Collins, T.E. Payne, T.D. Waite, Effect of amorphous Fe(III) oxide transformation on the Fe(II)-Mediated reduction of U(VI), Environ. Sci. Technol. 45 (2011) 1327–1333.
[59] L. Ling, W.-x. Zhang, Enrichment and encapsulation of uranium with iron nanoparticle, J. Am. Chem. Soc. 137 (2015) 2788–2791.
[60] Z.-J. Li, L. Wang, L.-Y. Yuan, C.-L. Xiao, L. Mei, L.-R. Zheng, J. Zhang, J.-H. Yang, Y.-L. Zhao, Z.-T. Zhu, Efficient removal of uranium from aqueous solution by zero-valent iron nanoparticle and its graphene composite, J. Hazard. Mater. 290 (2015) 26–33.
[61] S.R. Kanel, B. Manning, L. Charlet, H. Choi, Removal of arsenic(III) from groundwater by nanoscale zero-valent iron, Environ. Sci. Technol. 39 (2005) 1291–1298.
[62] T. Missana, M. García-Gutiérrez, V. Fernńdez, Uranium(VI) sorption on colloidal magnetite under anoxic environment: experimental study and surface complexation modelling, Geochim. Cosmochim. Ac. 67 (2003) 2543–2550.
[63] D. Das, M. Sureshkumar, S. Koley, N. Mithal, C. Pillai, Sorption of uranium on magnetite nanoparticles, J. Radioan. Nucl. Ch. 285 (2010) 447–454.
[64] A.F. White, M.L. Peterson, Reduction of aqueous transition metal species on the surfaces of Fe(II)-containing oxides, Geochim. Cosmochim. Ac. 60 (1996) 3799–3814.
[65] S. Yan, Y. Chen, W. Xiang, Z. Bao, C. Liu, B. Deng, Uranium(VI) reduction by nanoscale zero-valent iron in anoxic batch systems: the role of Fe(II) and Fe(III), Chemosphere 117 (2014) 625–630.
[66] G. Sheng, P. Yang, Y. Tang, Q. Hu, H. Li, X. Ren, B. Hu, X. Wang, Y. Huang, New insights into the primary roles of diatomite in the enhanced sequestration of UO_2^{2+} by zerovalent iron nanoparticles: an advanced approach utilizing XPS and EXAFS, Appl. Catal. B Environ. 193 (2016) 189–197.
[67] X. Jiang, Z. Ouyang, Z. Zhang, C. Yang, X. Li, Z. Dang, P. Wu, Mechanism of glyphosate removal by biochar supported nano-zero-valent iron in aqueous solutions, Colloids Surf. A 547 (2018) 64–72.
[68] Y. Zhang, Y. Su, X. Zhou, C. Dai, A.A. Keller, A new insight on the core–shell structure of zerovalent iron nanoparticles and its application for Pb(II) sequestration, J. Hazard. Mater. 263 (2013) 685–693.
[69] C. Mason, W. Turney, B. Thomson, N. Lu, P. Longmire, C. Chisholm-Brause, Carbonate leaching of uranium from contaminated soils, Environ. Sci. Technol. 31 (1997) 2707–2711.
[70] P. Zhou, B. Gu, Extraction of oxidized and reduced forms of uranium from contaminated soils: effects of carbonate concentration and pH, Environ. Sci. Technol. 39 (2005) 4435–4440.